Ground Support 2023 – J Wesseloo (ed.)

doi:10.36487/ACG_repo/2325_35

Numerical forecast of central access ground support behaviour at Cadia East PC1-2

E Ghazvinian *Itasca Consulting Group, Inc, USA*

C Orrego *Newcrest Mining Limited, Australia*

M Fuenzalida *Itasca Consulting Group, Inc, USA*

Abstract

The future PC1-2 block cave at Cadia East considers a central access to allow for a unique material handling system made up of two crusher chambers located at the northern and southern ends of the footprint. To implement this solution, a row of drawbells was removed from the mine design in the centre of the footprint, which creates a geotechnical singularity with the potential to be affected by increasing cave loading due to less interactive drawing on top of the central access, resulting in a stagnant zone formed above the drive. This stagnant zone is likely to attract stresses. This, in combination with the complex geometry of the super apices above the central access, increased the focus on long-term stability and the adequacy of the proposed ground support design; therefore, it was assessed using bonded block model (BBM) modelling with explicit ground support.

A BBM analysis was carried out to forecast support behaviour by explicitly representing the planned ground support in the model and its impact on the stability of the central access drive. The models simulated the process of excavating the drive, support installation, abutment loading and unloading, and lastly, cave loading to assess excavation stability and rock mass response in the vicinity of central access through the life of mine. This paper summarises the analysis, assumptions and outcomes of the study.

Keywords: *ground support, cave loading, bonded block model, forecast support behaviour*

1 Introduction

The future PC1-2 block cave at Cadia East considers a central access to allow for a unique material handling system made up of two crusher chambers located at the northern and southern ends of the footprint. To implement this solution, a row of drawbells was removed from the mine design in the centre of the footprint (Figure 1). This creates a geotechnical singularity with the potential to be affected by increasing cave loading due to less interactive drawing on top of the central access. The drawdown analysis indicated that material on top of the central access is mobilised at a slower rate compared to the other part of the cave, which will result in a stagnant zone forming above the drive. The presence of this stagnant zone is likely to attract stresses. This, in combination with the complex geometry of the super apices above the central access as well as strength degradation of the rock mass surrounding the drive during cave establishment and further on with cave loading, drew further attention to long-term stability and the adequacy of the ground support design. An advanced analysis was warranted to understand the rock mass response in the vicinity of the central access drive, focusing on forecasting excavation stability and ground support behaviour during cave establishment and cave loading, likely to occur during the cave production phase.

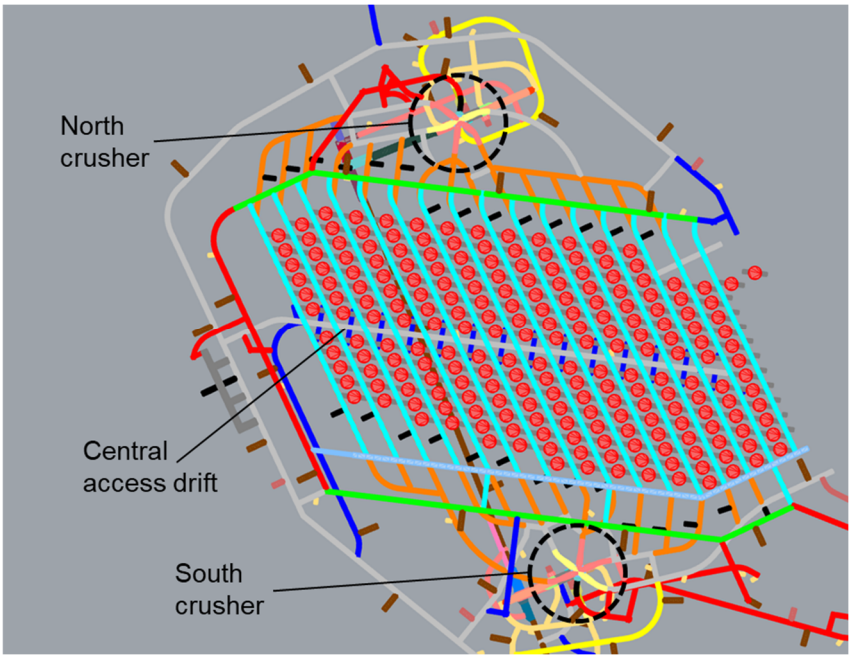

Figure 1 PC1-2 layout incorporating central access drive in the centre of the footprint (up is north)

2 Numerical approach

A detailed drive-scale 3D numerical model was constructed in *3DEC* (Itasca Consulting Group, Inc 2020) using the bonded block model (BBM) approach. The BBM model explicitly followed the geometry, in situ stress, simplified abutment loading/unloading and the subsequent cave loading for part of the central access away from the existing PC1-1 cave. The detailed representation of the excavation geometry, as shown in Figure 2, includes a BBM core surrounding an intersection of the central access with an extraction drive to capture the 3D nature of the loading condition. This BBM intersection is sandwiched by two intersections along the central access and two intersections along the extraction drive for proper boundary conditions. The external boundary of the model was constructed far from the BBM volume to allow for precise simulation of undercutting and cave-induced loads. The Itasca Constitutive Model for Advanced Strain Softening (IMASS) (Ghazvinian et al. 2020) was used outside the BBM domain for an accurate representation of rock mass response to stress changes and material recompaction (in the stagnant zone above the super apices). This ensures correct stress boundary conditions for the BBM part of the model.

The implementation of the BBM is used to represent the rock mass around the intersection, as it can simulate massive rock masses as bonded polyhedral elements that can break at their sub-contacts as a result of stress concentrations, mimicking the initiation of cracks that can coalesce and/or propagate to fracture the rock mass (Garza-Cruz & Pierce 2014). This results in an emergent damage pattern with associated unidirectional bulking around underground excavations. The ability to capture unidirectional bulking of the rock is instrumental for a reliable assessment of the deformation demand from ground support. The model provides predictions of rock mass response in the vicinity of the BBM intersection, as the undercut pass-over and cave propagation are simulated by simplifying assumptions. The resulting ground deformation and the emergent damage response would allow prediction of the excavation stability, as well as the expected ground support behaviour.

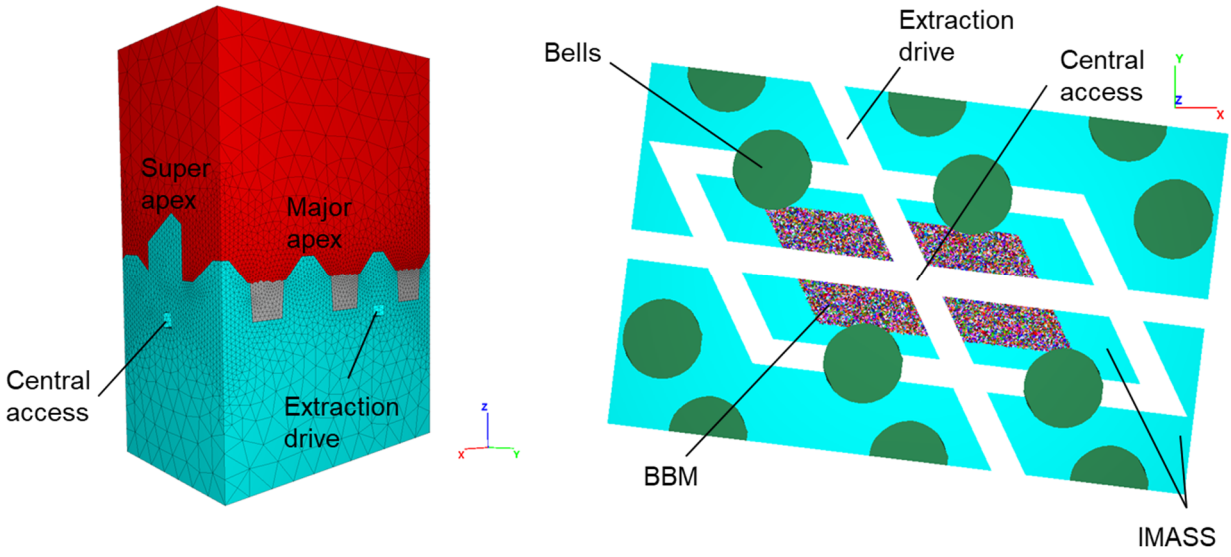

Figure 2 Model geometry. (a) Entire model domain; (b) Plan view mid-height of the drives (coloured blocks denote the BBM core)

2.1 Simulation sequence

Numerical simulation of cave establishment and propagation, especially when combined with BBM, can be computationally expensive. A staged approach was established to simulate abutment loading/unloading and the subsequent cave loading with a number of simplifying assumptions to minimise the computational overhead. A summary of the seven-stage modelling approach is schematically shown in Figure 3 and described:

- Stage 1: in situ stresses are initialised in the model.
- Stage 2: drives are excavated by incrementally relaxing the perimeter of the excavations and ground support is installed.
- Stage 3: the abutment loading is performed by applying a velocity boundary condition to the top of the model.
- Stage 4: blasting of the bells is simulated by converting the rock mass in the bells into broken rock with ~28% porosity (bulking = 0.4 in IMASS) and initialising their stresses to zero, then allowing the model to reach equilibrium and stresses to develop in the bells under gravity.
- Stage 5: simulation of unloading due to the formation of a destressed bowl near the intersection is performed by allowing the model to relax from the sides and its top boundary. Velocity boundary conditions control the relaxation rate for each principal stress to follow the anticipated stress path (see Section 2.2).
- Stage 6: the cave is initialised in the model following a similar approach described for the bells in Stage 4.
- Stage 7: cave loading is performed by incrementally increasing the applied stresses on top of the model. A scheme is activated in the background to constantly evaluate the stresses in the draw bells. Once the major principal stress for a drawbell zone reaches 1.0 MPa (stresses within the isolated movement zone are relatively low due to the significant amount of arching within a flow zone; Pierce 2019), the function resets the stresses for that zone to zero. This scheme was used to represent production and allow for stresses to arch above the draw bells.

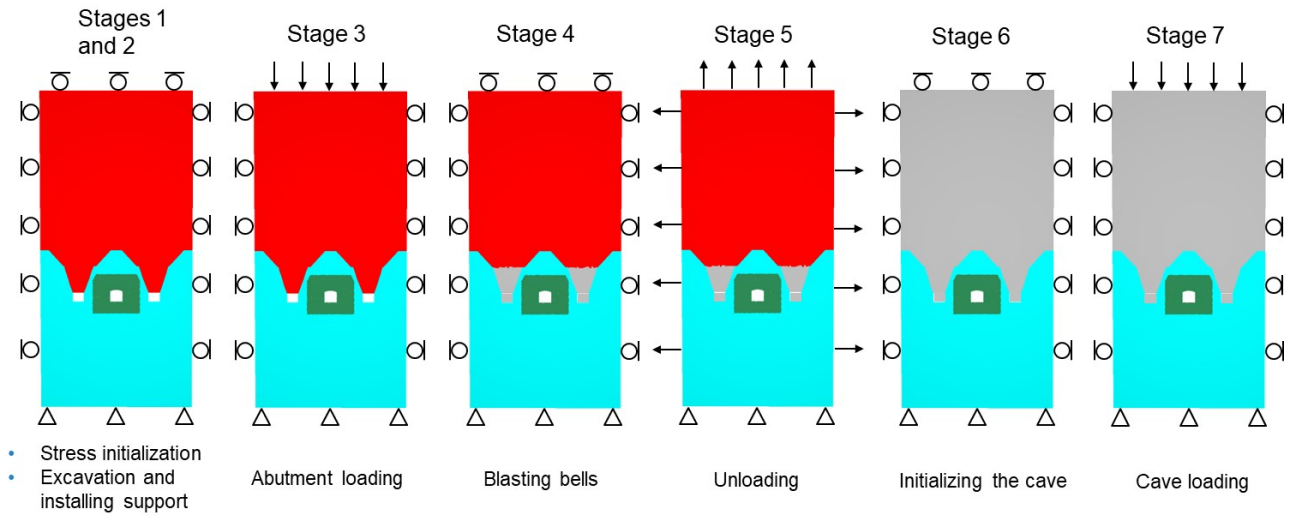

Figure 3 Seven-stage simulation sequence to represent the effect of cave establishment and propagation on the central access

2.2 Loading path

The stress path the central access pillar experiences during cave establishment and propagation can be complex and controlled by numerous factors, such as draw rate or differential draw rates from neighbouring bells. One of the main simplifying components of the BBM analysis was streamlining the loading path for the model. The anticipated stress path within the pillar between the intersection and the undercut drive during abutment loading and unloading was established from the results of a *FLAC3D* (Itasca Consulting Group, Inc 2019) model that explicitly represented the excavation of the drives, blasting of the bells and undercut development. The simplified loading path is shown in Figure 4. Pre-mining stresses reflect the Cadia East stress tensor, away from the influence of the existing PC1-1 cave (Sig 1 and Sig 2 are horizontal and trending 74 and 164° respectively, Sig 3 is vertical – central access runs nearly east–west). The effect of undercutting was indirectly captured in the BBM model by following this loading path (represented in the stresses captured from the *FLAC3D* model).

The simplified loading path was used to guide the model during the loading and unloading stages of the simulation, as described in Section 2.1. It should be noted that the stresses prior to the cave loading path in Figure 4 characterise the anticipated stresses in the central access pillar, whereas cave load is the average stress felt by the undercut level. The stresses induced in the central access pillar and its vicinity due to cave loading are significantly different from the cave load due to the points raised in the introduction (the stagnant zone above central access, complex geometry and strength degradation) that essentially define the purpose of this study.

Based on Janssen's (1895) bin theory, and consistent with the results of the PC1-2 caving analysis, the average cave load across the footprint of PC1-2 when the cave is established will be within a 5–10 MPa range. The cave loading in this study was continued up to 25 MPa to account for extension of the stagnant zone above the central access to higher elevations with continued production, which, in return, will attract higher stresses. The models suggest that 70–80 MPa stresses are developed in the central access pillar at a cave load of approximately 25 MPa. This is consistent with the conservative stresses calculated in a first pass stability analysis considering a local extraction ratio (ER) of 42% for the central access pillar (assuming a drawpoint spacing of 32 × 20 m) to convert vertical stresses acting on the stagnant zone (calculated using the tributary area method from vertical stresses acting on sectors north and south of the central access) to the stress induced on the central access.

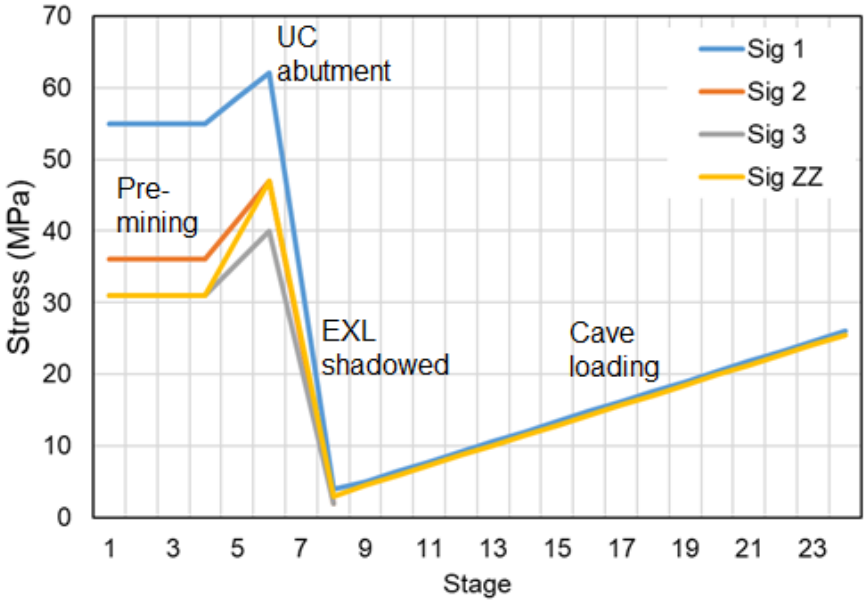

Figure 4 Simplified loading path used in the analysis

2.3 Rock mass strength

In the BBM modelling approach, the emergent material behaviour is not explicitly specified. Instead, the properties of the bonds are populated based on field data to result in emergent field-scale material properties and behaviour. Figure 5 displays the heterogeneity in rock mass strength captured using this methodology. More detail on the BBM approach can be found in Garza-Cruz & Pierce (2014). To use BBM to analyse the central access stability, the BBM strength was based on systematic point load test (PLT) data.

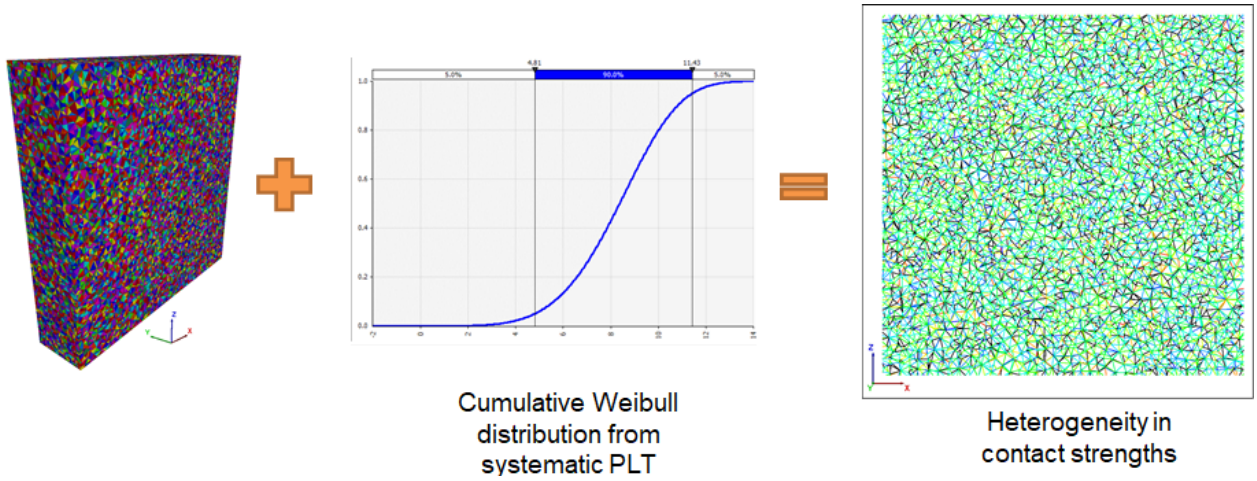

Figure 5 BBM construction

Cadia has an extensive database of PLT data covering a large extent of the PC1-2 footprint from systematic borehole logging and the subsequent machine learning study. A description of the geotechnical block model for Cadia is given in Pierce et al. (2022) and typical ranges of rock mass strength at different scales for Cadia are reported in Fuenzalida et al. (2022). Based on the distribution of Weibull PLT data parameters (rolling average within 30 m window) along the boreholes in the vicinity of the central access, a set of parameters was selected to be representative of a large extent of the central access based on the geotechnical block model. The Weibull fit parameters are 4.5 MPa for characteristic Is50 (63rd percentile of distribution) and 1.6 for shape factor, including 15% zeros (PLTs on open features). A summary of the BBM properties used in the current analysis is presented in Table 1.

The friction angles for the contacts between bonded blocks were determined mainly from back-calculation of the available triaxial compressive strength test database for Cadia. This back-calculation suggested friction angles around 45° for intact contacts. This value is used for the base case in the current study. In addition, a pessimistic case is analysed whereby the friction is reduced to 30°, and the dilation angle is adjusted accordingly, consistent with frictional properties of weak veins (Is50 < ~1 MPa) from benchmarking of similar ore deposits. The corresponding spalling strengths using 45 and 30° friction angles are approximately 22 and 12.5 MPa, as shown in Figure 6.

Table 1 Calibrated and PLT-driven BBM properties

Block properties		
Young's modulus	40.0 GPa	
Poisson's ratio	0.25	
Density	2,800 kg/m^3	
Contact properties		
Contact	**Intact**	**Zero strength**
Constitutive model	Mohr–Coulomb	Mohr–Coulomb
Normal stiffness	235 GN/m	235 GN/m
Shear stiffness	117.5 GN/m	117.5 GN/m
Peak friction angle	45° (30°*)	60° (30°*)
Residual friction angle	45° (30°*)	60° (30°*)
Dilation angle	15° (10°*)	30° (10°*)
Peak tensile strength	Randomly sampled from intact Weibull distribution	0
Residual tensile strength	0	0
Peak cohesive strength	2.5 × tensile strength	0
Residual cohesive strength	0	0
Emergent rock mass properties		
Young's modulus	~21 GPa (corresponding to volcanics with GSI = 60)	
Large-scale in situ strength (spalling)	22 MPa (12.5 MPa*)	

*Pessimistic case

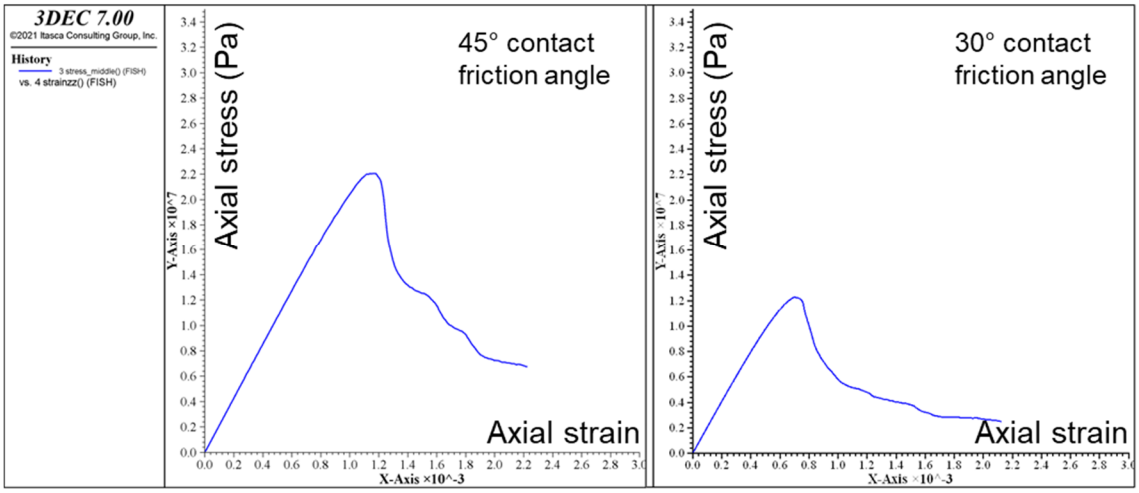

(a) (b)

Figure 6 Spalling strength for (a) Base case and (b) Pessimistic case

2.4 Support elements

The proposed support design to be evaluated is described in this section. The support layout for the central access drive includes (Figure 7a):

- 50 mm fibre-reinforced shotcrete (FRS) – floor-to-floor.
- Minax mesh.
- 3.0 m Posimix bolts (1.3 × 1.3 m spacings):
  - 20 mm diameter.
  - 1.4 m de-bonded.
- 6.2 m single strand (17.8 mm), fully grouted cable bolts (1.3 × 1.3 m spacings in backs).
- 4.5 m single strand (17.8 mm), fully grouted cable bolts (1.3 × 1.3 m spacings in walls).

The support design for extraction drives (EXT) includes (Figure 7b):

- 50 mm FRS – floor-to-floor.
- Minax mesh.
- 2.4 m Posimix bolts (1.3 × 1.3 m spacings):
  - 20 mm diameter.
  - 1.4 m de-bonded.
- 4.5 m single strand (17.8 mm), fully grouted cable bolts (2.6 × 2.6 m spacings in backs and shoulders).

The Posimix bolts and single strand cables were explicitly represented in the model. The FRS and Minax mesh were not included in the analysis in a conservative simplification. The hybrid bolts in *3DEC* (Bouzeran et al. 2017) were used to represent the Posimix bolts and single strand cables. The hybrid bolt is a one-dimensional reinforcement element designed to simulate a rockbolt in a jointed rock or fractured ground. Posimix bolt properties were calibrated to mimic the force/displacement response of a 20 mm resin grouted rockbolt in laboratory pull and shear tests (Stjern 1995). They can sustain 160 kN of axial force in tension and undergo ~21% of axial strain before rupturing. In the absence of any available laboratory pull and shear tests for 17.8 mm cables, the properties of this support element were calibrated based on the load capacity (330 kN) and assuming displacement behaviour consistent with 15.2 mm cables for which lab data is available and a

rupturing strain of ~17.5% (Stjern 1995). The dowel strength was conservatively assumed to be equal to the axial yield strength.

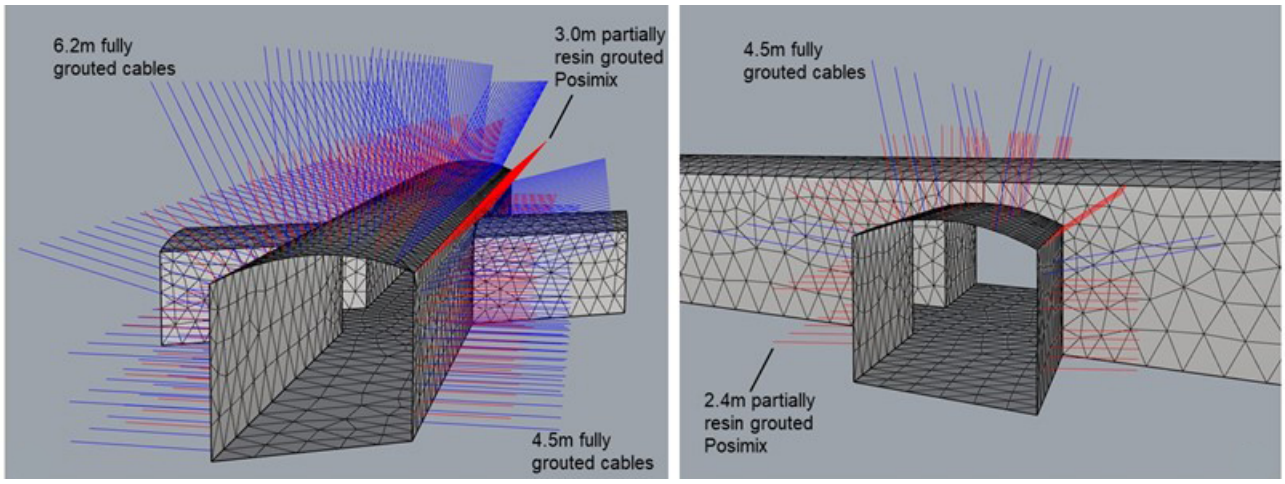

(a) (b)

Figure 7 Support design for: (a) Central access drive; (b) EXT drives

3 Central access forecasted behaviour

Modelled damage and fracturing of the rock mass near the central access is shown in Figure 8 in plan view at mid-height of the drives at various stages of cave establishment and propagation for the base case and pessimistic case. In these plots, broken contacts, representing cracks, are shown with black lines. Those contacts are slipping or have slipped in the past and only have frictional strength. Blocks (fragments) with different colours are completely disconnected from their surroundings and frictional-only strength is governed by their contacts.

The model forecasts minimal excavation-induced fracturing and slabbing in the walls and floor of the central access for the base case. The fracturing is sporadic in the backs due to the arch shape. Abutment loading increases the damage in the floor and walls. However, a large increase in the depth of damage surrounding the central access (walls, floor and backs) is associated with the unloading event (stress shadowing of the extraction level and formation of a destressed bowl). This is due to the accelerated reduction in minor principal stress compared to the major principal stress in the tunnel periphery during unloading, which results in a localised stress path intersecting with the rock mass peak strength envelope (therefore, fracturing of the rock).

The rock mass damage is more extensive for the pessimistic case. The fracturing in the walls, backs and floor is observed to continuously grow during abutment loading and unloading as well as during the cave loading phase. The ground support is, however, effective in maintaining confinement in the backs and walls of the drive and minimising the relaxed zone (an indicator for depth of damage measured in the field), as shown with contours of Sig 1 in Figure 9. The damage incurred to the corners of the super apex during cave loading can be seen in the same figure. The depth of the relaxed zone in the walls at 25 MPa cave loading is shown in Figure 10, ranging between 1 and 1.5 m, reducing the effective pillar width.

It should be noted that the impact of stress changes on the grout strength of cable bolts (Hutchinson & Diederichs 1996) is not considered in this study. Previous experiences at Cadia do not raise major concerns in this regard. In addition, the unsupported cases that were simulated in parallel (replicating extreme sensitivity of grout strength to stress reduction) showed greater convergence for walls and backs but no changes in the integrity of the system. This is discussed in the next section.

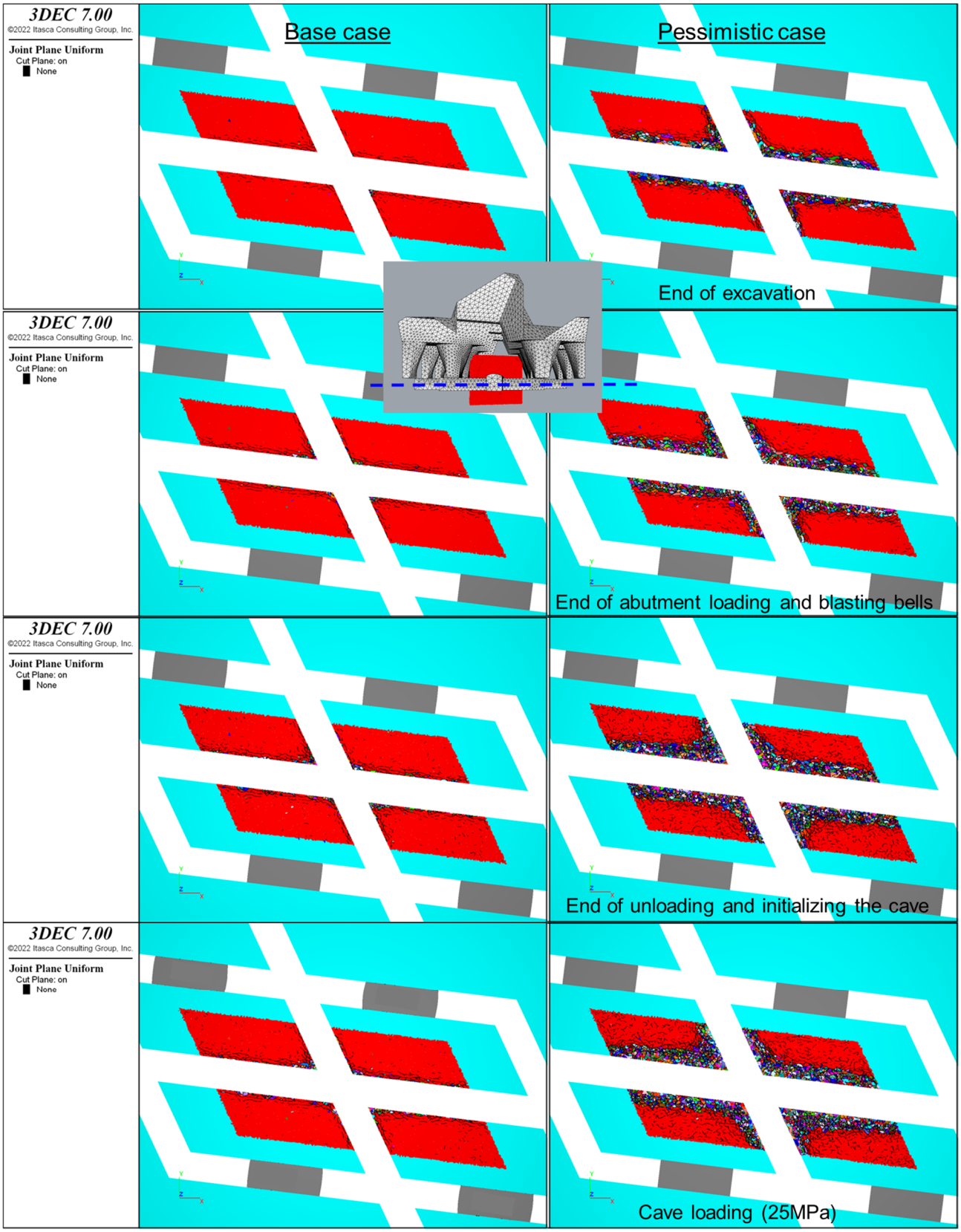

Figure 8 Damage and fracturing at various stages of cave establishment and cave loading (plan view mid-height of the drives)

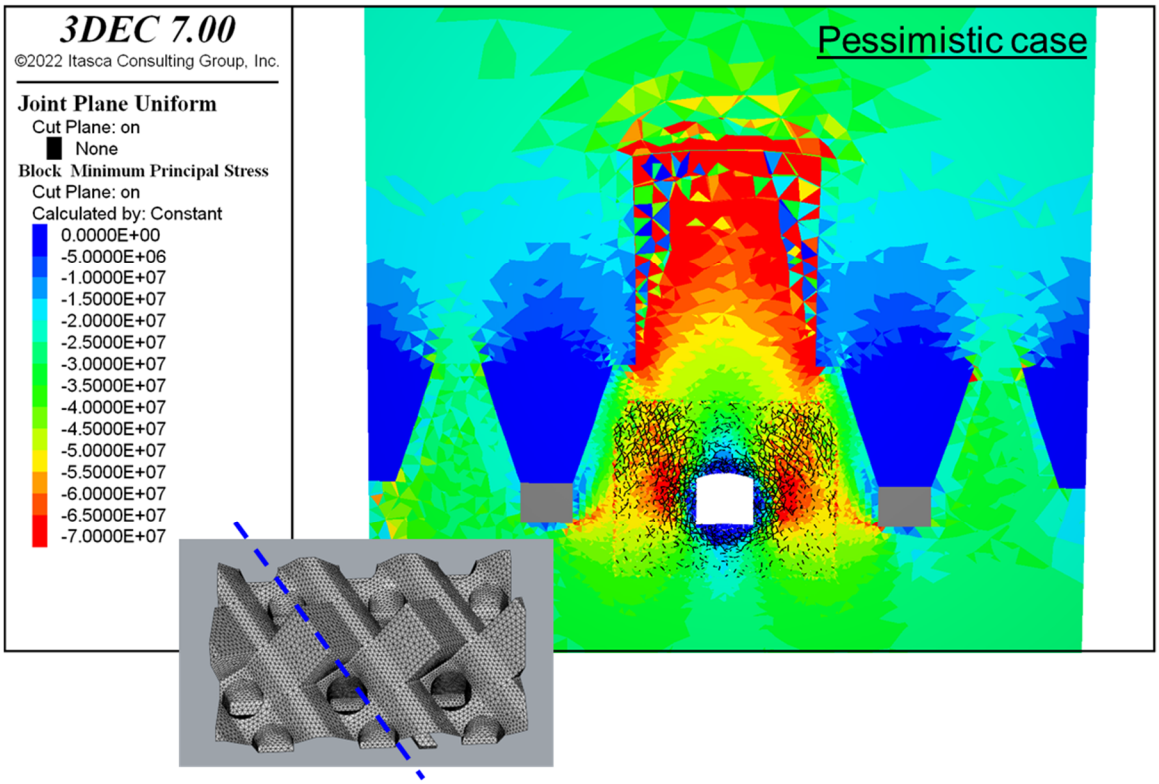

Figure 9 Contour of major principal stress at the end of cave loading – 25 MPa for the pessimistic case (cut plane through the super apex)

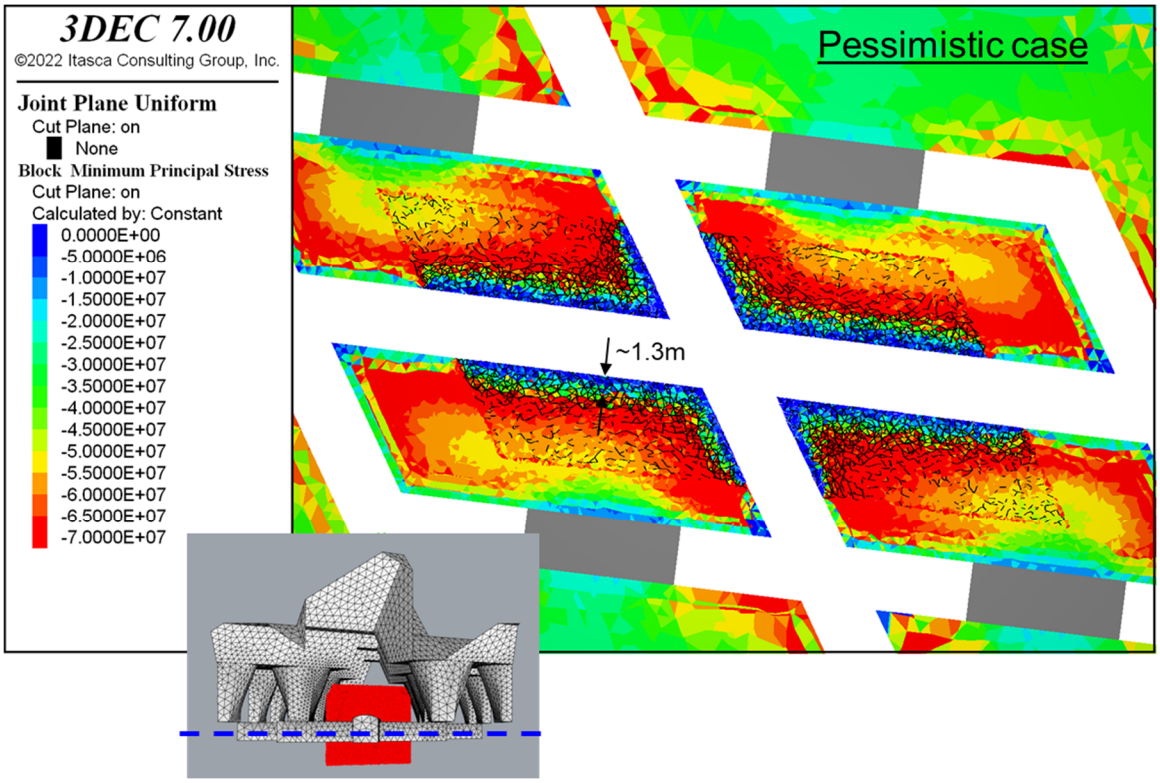

Figure 10 Contour of major principal stress at the end of cave loading – 25 MPa for the pessimistic case (plan view mid-height of the drives)

4 Ground support modelling results

The more intense fracturing in the pessimistic case puts a higher demand on the support; therefore, the results of that scenario are discussed in this section. Overall, the model predicts that the maximum support demand in the central access drive back occurs at the end of abutment loading and blasting of the bells. The demand in this area decreases through the unloading and cave loading phases. On the other hand, the axial force capacity of the cable bolts is fully exercised within the fractured parts of the walls at those two stages (see the top of Figure 11). During cave loading, bulking of the fractured rock within the inner periphery of the drive consumes part of the axial strain capacity of the cable bolts (up to around 4–6%), as shown in the bottom of Figure 11, leaving a good margin for the axial strain capacity (up to 17.5%). A localised axial rupture is observed in one of the cables (Figure 11), but this is not a systematic pattern observed along the central access drive. The axial forces in Posimix bolts at the end of cave loading are around 140 kN (below their maximum tensile capacity) due to their unbonded length.

To quantify the impact of ground support in controlling the drive walls and back deformation, virtual extensometers of 5 m in length were installed in the periphery of the drive, as shown in Figure 12. The nodes of these extensometers are 0.5 m apart and measure the deformation relative to the anchor at the end of the hole. The measured convergence at maximum cave loading (25 MPa) places the central access drive at level 2 (40–80 mm convergence) of the Cadia East geotechnical excavation management trigger action response plan (TARP), indicating that preventive support maintenance will be required during the life of mine. In the absence of any ground support (unsupported case in the same figure), the modelled walls and backs move more than 120 mm – consistent with level 4 of the Cadia East TARP. Assuming fracturing in the walls is concentrated within 1.5 m depth near the excavation (observed for excavations with similar conditions at Cadia East), a bulking factor ranging between 7 and 11% can be estimated for the unsupported drive. Adding support reduces the bulking to a narrower range between 4 and 5%.

Comparing drive wall convergence between supported and unsupported models in Figure 11 shows insignificant differences at measurement locations near the floor. The virtual extensometers at those locations were installed 0.5 m from the floor in close proximity to the lower wall cables. Assessment of axial force and axial strain in cables on a representative vertical section along the central access drive at the end of cave loading (25 MPa) indicated a relatively small contribution of the lower wall cables to wall movement and, therefore, an opportunity for optimising the design. It should be noted that this assessment does not consider the role those cables can play in drive stability in the case of a dynamic event during abutment loading.

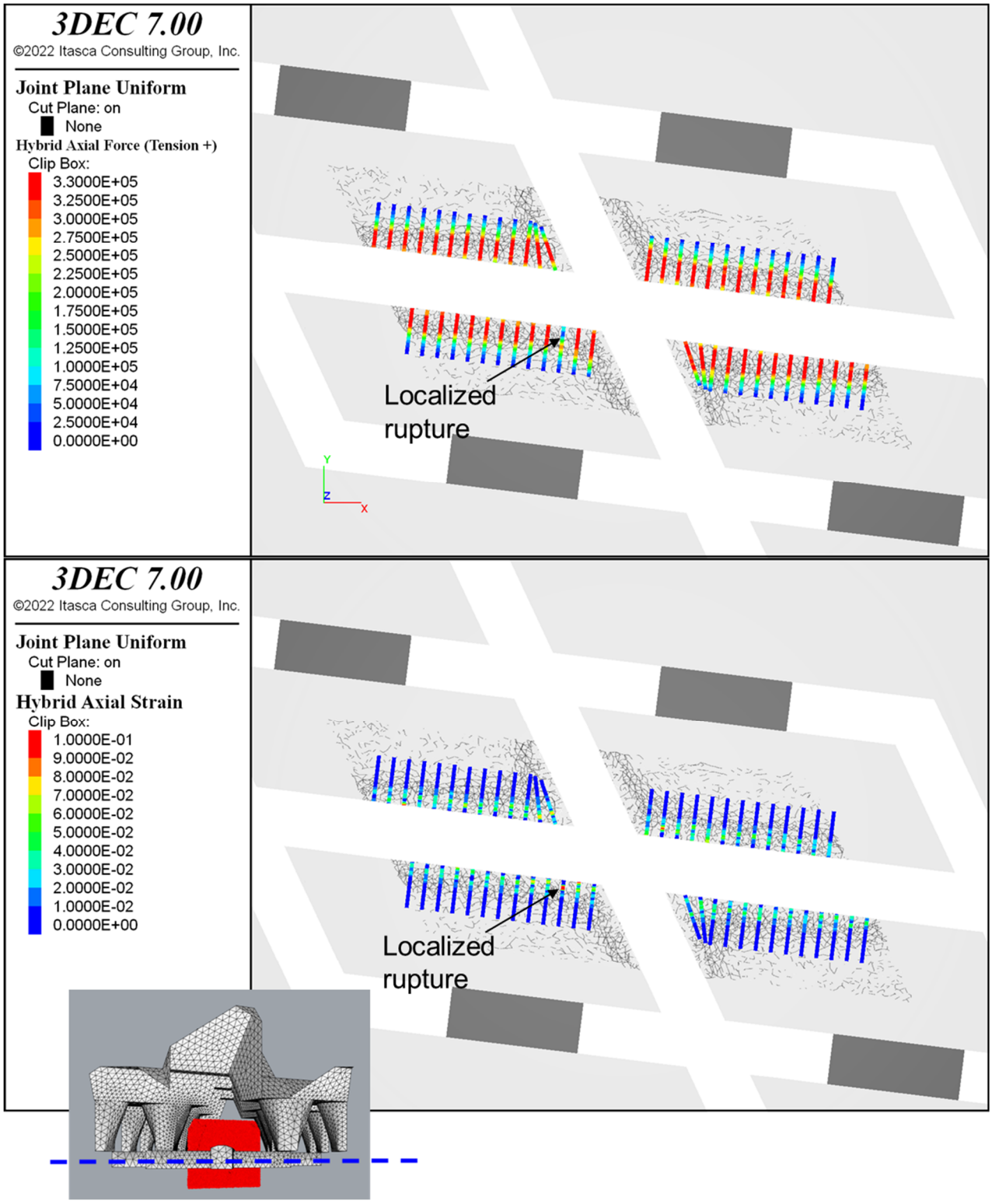

Figure 11 **Top: contour of axial force in the cable bolts installed mid-height of the drives (maximum force capacity of cable bolts is 330 kN). Bottom: contour of axial strain (maximum axial strain capacity for the cable bolts is 0.175), at the end of cave loading (25 MPa) for the pessimistic case**

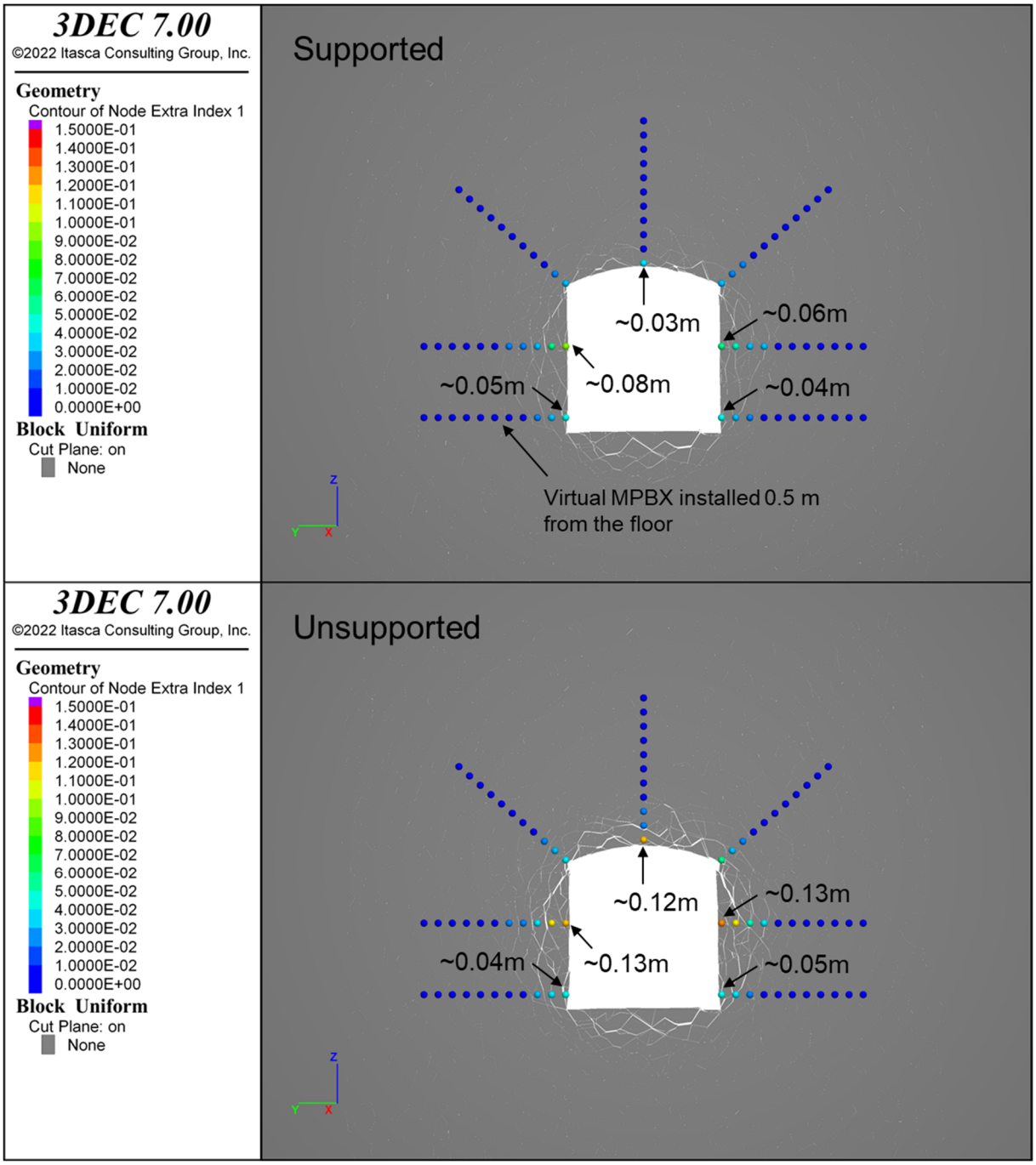

Figure 12 Contour of central access drive deformation measured along the direction of installed virtual extensometers at the end of cave loading (25 MPa) for the pessimistic case

5 Conclusion

The drive stability and support behaviour were analysed for the PC1-2 central access through the life of mine. The methodology described in this study to isolate a representative section of a cave mine footprint with symmetrical boundary conditions would allow for detailed representation of drive excavation, support installation and complex stress changes surrounding the drive throughout the cave establishment phase, including abutment loading and unloading and subsequent cave loading without much computational overhead. These efficient models lend themselves to discontinuum modelling approaches such as BBM. The implementation of BBM to represent the rock mass around the excavations can simulate massive rock masses as bonded polyhedral elements that can break at their contacts as a result of stress concentrations, mimicking the initiation of cracks that can coalesce and/or propagate to fracture the rock mass. This results

in an emergent damage pattern with associated bulking. The unidirectional bulking around excavations, emergent in this technique, is key to capturing the correct support response and a reliable assessment of the deformation demand from ground support. The resulting ground deformation and the emergent damage response would allow prediction of excavation stability and optimisation of ground support design.

Acknowledgement

The authors thank Newcrest Mining Limited for allowing publication of this paper.

References

Bouzeran, L, Furtney, J, Pierce, M, Hazzard, J & Lemos, JV 2017, 'Simulation of ground support performance in highly fractured and bulked rock masses with advanced 3DEC bolt model', in J Wesseloo (ed.), *Deep Mining 2017: Proceedings of the Eighth 'International Conference on Deep and High Stress Mining*, Australian Centre for Geomechanics, Perth, pp. 667–680, https://doi.org/10.36487/ACG_rep/1704_45_Bouzeran

Fuenzalida, MA, Orrego, C, Ghazvinian, E & Pierce, ME 2022, 'Application of rock mass strength scale effect at Cadia East mine', in Y Potvin (ed.), *Caving 2022: Fifth International Conference on Block and Sublevel Caving, Australian Centre for Geomechanics*, Perth, pp. 951–962, https://doi.org/10.36487/ACG_repo/2205_65

Garza-Cruz, TV & Pierce, M 2014, 'A 3DEC model for heavily veined massive rock masses', *Proceedings of the 48th US Rock Mechanics/Geomechanics Symposium*, ARMA 14-7660, American Rock Mechanics Association, Alexandria.

Ghazvinian, E, Garza-Cruz, T, Bouzeran, L, Fuenzalida, M, Cheng, Z, Cancino, C, & Pierce, M 2020, 'Theory and implementation of the Itasca Constitutive Model for Advanced Strain Softening (IMASS)', *MassMin 2020: Proceedings, Eighth International Conference & Exhibition on Mass Mining*, pp. 451–461, University of Chile, Santiago.

Hutchinson, DJ & Diederichs, MS 1996, *Cablebolting in Underground Mines*. Bitech Publishers Ltd, Vancouver.

Itasca Consulting Group, Inc 2019, *FLAC3D — Fast Lagrangian Analysis of Continua in Three Dimensions*, version 7.0, computer software, Itasca Consulting Group, Inc, Minneapolis.

Itasca Consulting Group, Inc 2020, *3DEC — Three-Dimensional Distinct Element Code*, version 7.0, computer software, Itasca Consulting Group, Inc, Minneapolis.

Janssen, HA 1895, 'Experiments regarding grain pressure in soils', *Zeitschrift Des Vereines Deutscher Ingenieure*, vol. 39, no. 35, pp. 1045–1049, translated from German by W Hustrulid & N Krauland, in A Karzulovic & MA Alfaro (eds), *Proceedings of MassMin 2004: Proud to be Miners*, Mineria Chilena, Santiago, pp. 201–214.

Pierce, M 2019, 'Forecasting vulnerability of deep extraction level excavations to draw-induced cave loads', *Rock Mechanics and Geotechnical Engineering*, vol. 11, no. 3.

Pierce, ME, Stonestreet, P, Orrego, C, Tennant, D, Garza-Cruz, TV, Furtney, J & Thielsen, C 2022, 'Development of rock mass strength block models at Cadia East mine', in Y Potvin (ed.), *Caving 2022: Fifth International Conference on Block and Sublevel Caving*, Australian Centre for Geomechanics, Perth, pp. 1033–1046, https://doi.org/10.36487/ACG_repo/2205_71

Stjern, G 1995, *Practical Performance of Rock Bolts*, PhD thesis, University of Trondheim, Trondheim.